

**Dissipative dynamics of a particle in a vibrating periodic potential: Chaos and control**R. Chacón,<sup>1</sup> P. J. Martínez,<sup>2</sup> and J. A. Martínez<sup>3</sup><sup>1</sup>*Departamento de Física Aplicada, E.I.I., Universidad de Extremadura, Apartado Postal 382, E-06006 Badajoz, Spain and Instituto de Computación Científica Avanzada, Universidad de Extremadura, E-06006 Badajoz, Spain*<sup>2</sup>*Departamento de Física Aplicada, E.I.N.A., Universidad de Zaragoza, E-50018 Zaragoza, Spain and Instituto de Ciencia de Materiales de Aragón, CSIC-Universidad de Zaragoza, E-50009 Zaragoza, Spain*<sup>3</sup>*Departamento de Ingeniería Eléctrica, Electrónica y Automática, Escuela de Ingenierías Industriales, Universidad de Castilla-La Mancha, E-02071 Albacete, Spain*

(Received 27 May 2015; revised manuscript received 22 September 2015; published 23 December 2015)

The dissipative chaotic dynamics of a particle subjected to a horizontally vibrating periodic potential is characterized theoretically and confirmed numerically in the case of an external chaos-controlling periodic excitation also acting on the particle. Theoretical predictions concerning the chaotic threshold in parameter space are deduced from the application of Melnikov's method that fully determine the chaos-control scenario. Also, the structure of diverse regularization regions in parameter space is explained theoretically with the aid of an energy analysis. It was found that the phase difference between the two periodic excitations involved plays a crucial role in the chaos-control scenario, with the particular feature that its optimal value depends upon the ratio between the damping coefficient and the excitation frequency. This constitutes a genuine feature of the chaos-control scenario associated with nonsteady potentials which is in contrast to the case of steady potentials. Additionally, we demonstrate the robustness of the chaos-control scenario against the presence of low-intensity Gaussian noise and reshaping of chaos-suppressing excitations.

DOI: [10.1103/PhysRevE.92.062921](https://doi.org/10.1103/PhysRevE.92.062921)

PACS number(s): 05.45.Gg, 05.45.Xt

**I. INTRODUCTION**

The dynamical outputs of a complex nonlinear system in response to external excitations are of both fundamental theoretical relevance and practical interest. In particular, the application of judiciously chosen periodic external excitations constitutes a universal procedure to control chaos in general systems. The present work studies the chaotic dissipative dynamics of a particle subjected to a horizontally vibrating periodic potential and driven by an external periodic excitation according to the model equation

$$\ddot{x} + \sin[x - f(t)] = -\delta\dot{x} + F(t), \quad (1)$$

where  $f(t)$  and  $F(t)$  are periodic functions while  $\delta$  is the damping coefficient, with particular emphasis on the suppressory effect of the external excitation  $F(t)$  on the chaos induced by the horizontally vibrating periodic potential

$$V(x, t) = 1 - \cos[x - f(t)]. \quad (2)$$

Diverse versions of the dimensionless Eq. (1) arise in many physical contexts, such as the chaotic phase oscillation of a proton beam in a cooler synchrotron [1,2], the dynamics of a cylindrical pinion that is kept at a distance from a sinusoidally vibrating rack while the two are coupled by the lateral Casimir force [3], and the dynamics of a bright soliton appearing in a Bose-Einstein condensate in a horizontally vibrating shallow optical lattice [4]. Phase modulation of periodic potentials has also been considered in the wave equation describing beam propagation in a periodically curved waveguide array [5], as well as in studies of Wannier-Stark resonances in optical and semiconductor superlattices [6]. Also, there have been studies of coupled systems of particles subjected to horizontally vibrating periodic potentials. A case is that of repulsively, power-law interacting particles in one dimension [7]. When the presence of dissipation is unavoidable, the consideration of

chaos-suppressing (CS) excitations  $F(t)$  is especially pertinent since it means the possibility of complete regularization of the dynamics in the whole phase space over finite regions of parameter space [8]. This is the case, for example, of the aforementioned nanoscale noncontact rack-and-pinion setups [3] as well as the formation of vortices in a Bose-Einstein condensate [9]. To the best of the authors' knowledge, the general chaos-control scenario described by Eq. (1) has not as yet been investigated.

Here we undertake theoretical and numerical studies of this new chaos-control scenario by focusing on the simple case in which the two time-periodic functions involved are harmonic and satisfy a simple resonance condition. The remainder of the communication is organized as follows. Section II studies the chaotic dynamics arising from Eq. (1) in the absence of any CS excitation. Analytical estimates of the chaotic threshold in parameter space are obtained by using Melnikov's method (MM) while numerical experiments provide confirmation of the theoretical predictions. Also, the structure of diverse nonchaotic regions arising beyond the chaotic threshold in parameter space is explained theoretically with the aid of an energy analysis. The effectiveness and robustness of resonant harmonic excitations  $F(t)$  at suppressing the chaos induced by the sinusoidally vibrating periodic potential is demonstrated theoretically and confirmed numerically in Sec. III. Finally, Sec. IV is devoted to a discussion of the major findings and of some open problems.

**II. VIBRATING-POTENTIAL-INDUCED CHAOS**

We shall concentrate in this section on the chaotic behavior induced by a horizontally and sinusoidally vibrating potential in the absence of any CS excitation,

$$\ddot{x} + \sin[x - \gamma \cos(\omega t)] = -\delta\dot{x}, \quad (3)$$

which is equivalent to

$$\ddot{\theta} + \sin \theta = -\delta \dot{\theta} + \delta \gamma \omega \sin(\omega t) + \gamma \omega^2 \cos(\omega t), \quad (4)$$

$$\theta(t) \equiv x(t) - \gamma \cos(\omega t), \quad (5)$$

where  $\theta$  and  $x$  are the particle phases relative to the vibrating potential frame and the laboratory frame, respectively. Note that Eq. (5) tells us that chaotic dynamics may be equivalently studied in any of such frames. Thus, to obtain analytical estimates of the chaotic threshold in parameter space  $(\gamma, \omega, \delta)$ , we assume that system (4) satisfies the MM requirements, i.e., the dissipation and excitation terms are small-amplitude perturbations of the underlying conservative pendulum  $\ddot{\theta} + \sin \theta = 0$ .

### A. Melnikov's method predictions

Melnikov introduced a function [now known as the Melnikov function (MF),  $M(t_0)$ ] which measures the distance between the perturbed stable and unstable manifolds in the Poincaré section at  $t_0$ . If the MF presents a simple zero, the manifolds intersect transversally and chaotic instabilities result. See Refs. [10,11] for more details about MM. Regarding Eq. (4), note that keeping with the assumption of the MM [10,11], it is assumed that one can write  $\delta = \varepsilon \bar{\delta}, \gamma = \varepsilon \bar{\gamma}$ , where  $0 < \varepsilon \ll 1$  while  $\bar{\eta}, \bar{\gamma}, \omega$  are of order one. This means that the term  $\delta \gamma \omega \sin(\omega t)$  in Eq. (4) is  $O(\varepsilon^2)$  and one should drop it to calculate the MF. However, it will be kept in calculating the MF to obtain a reliable estimate of the chaotic threshold in parameter space since nonperturbative values of the parameters were used in the numerical experiments. Thus, bearing in mind this caveat, the application of MM to Eq. (4) yields the MF

$$\begin{aligned} M^\pm(t_0) &= -D \pm A \cos(\omega t_0) \pm B \sin(\omega t_0), \\ D &\equiv 8\delta, \\ A &\equiv 2\pi \gamma \omega^2 \operatorname{sech}(\pi \omega / 2), \\ B &\equiv 2\pi \gamma \delta \omega \operatorname{sech}(\pi \omega / 2), \end{aligned} \quad (6)$$

where the positive (negative) sign refers to the top (bottom) homoclinic orbit of the underlying conservative pendulum

$$\begin{aligned} \theta_0(t) &= \pm 2 \arctan[\sinh(t)], \\ \dot{\theta}_0(t) &= \pm 2 \operatorname{sech}(t). \end{aligned} \quad (7)$$

Note that  $A \cos(\omega t_0) + B \sin(\omega t_0) \leq \sqrt{A^2 + B^2}, \forall t_0$ , and hence the relationship

$$D \geq \sqrt{A^2 + B^2} \quad (8)$$

represents a sufficient condition for  $M^\pm(t_0)$  to be negative (or null) for all  $t_0$ . Therefore, a necessary condition for the occurrence of a homoclinic bifurcation and the subsequent chaotic instabilities is  $D < \sqrt{A^2 + B^2}$  or [cf. Eq. (6)]

$$\gamma > \gamma_{th} = \gamma_{th}(\delta, \omega) \equiv \frac{4\delta \cosh(\pi \omega / 2)}{\pi \omega \sqrt{\delta^2 + \omega^2}}, \quad (9)$$

where  $\gamma_{th}$  is the threshold amplitude providing an estimate of the boundary of the region in parameter space in which homoclinic chaos occurs (see Fig. 1). We now compare

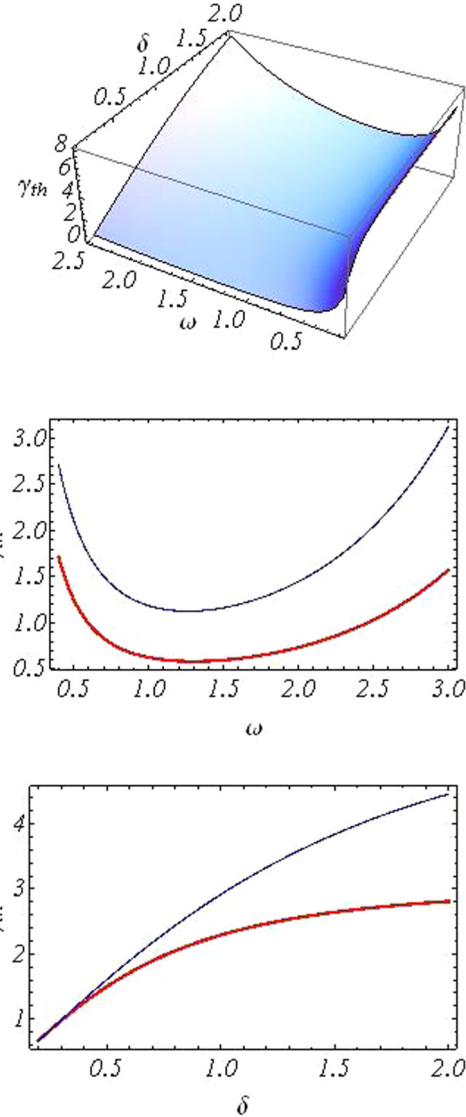


FIG. 1. (Color online) Plots of the chaotic threshold amplitude  $\gamma_{th}$  [see Eq. (9)]. Top panel:  $\gamma_{th}$  vs  $\omega$  and  $\delta$ . Middle panel:  $\gamma_{th}$  vs  $\omega$  for  $\delta = 0.4$  (thin line) and  $\delta = 0.2$ . Bottom panel:  $\gamma_{th}$  vs  $\delta$  for  $\omega = 1.8$  (thin line) and  $\omega = 0.9$ . The quantities plotted are dimensionless.

the theoretical prediction obtained from MM (recall the aforementioned caveat) with the Lyapunov exponent (LE) calculations for Eq. (2). Computer simulations of Eq. (2) showed that MM-based predictions provide useful quantitative information regarding the onset of chaos even when the values of the excitation amplitude  $\gamma$  and damping coefficient  $\delta$  do not reasonably satisfy the MM requirements [10,11]. In this regard, it is worth recalling that, even in the case of small values of  $\gamma$  and  $\delta$ , one cannot expect too good a quantitative agreement between these two kinds of approaches because MM is a perturbative technique generally related to transient chaos, while LE provides information solely concerning steady responses. We computed the LEs using a version of the algorithm introduced in Ref. [12], with integration typically up to  $10^4$  drive cycles for each fixed set of parameters. The numerical results confirmed the effectiveness of the estimation procedure (9). This unreasonable effectiveness of

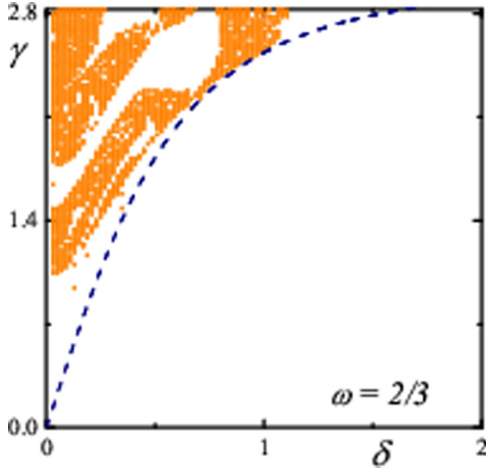


FIG. 2. (Color online) Chaotic regions (dots) in the  $\delta$ - $\gamma$  parameter plane corresponding to Eq. (3) for  $\omega = 0.67$ . A dot is plotted on a  $100 \times 140$  grid when the corresponding maximal LE is larger than  $10^{-3}$ . The line represents the theoretical chaotic threshold [cf. Eq. (9)].

MM predictions beyond the perturbative regime has previously been reported in diverse contexts (see, e.g., Ref. [8]). An illustrative example is shown in Fig. 2, where one sees how the chaotic regions in the  $\delta$ - $\gamma$  parameter plane are reasonably well bounded by the estimate (9). Worth noting, however, is the existence of regularization islands inside the global chaotic region in the  $\delta$ - $\gamma$  parameter plane, which cannot be explained from MM. The following subsection presents an energy-based analysis providing such an explanation.

### B. Energy-based analysis

By analyzing the variation in the system's energy, one can obtain useful information about the structure of chaotic and nonchaotic regions in parameter space. Indeed, Eq. (2) has the associated energy equation

$$\dot{E} = \dot{x} \cos(x) \sin[\gamma \cos(\omega t)] - \delta \dot{x}^2 + 2\dot{x} \sin(x) \sin^2\left[\frac{\gamma}{2} \cos(\omega t)\right], \quad (10)$$

where  $E(t) \equiv (1/2)\dot{x}^2(t) + U[x(t)]$  [ $U(x) \equiv 1 - \cos x$ ] is the energy function. Integration of Eq. (10) over *any* interval  $[nT, nT + T/2]$  ( $T \equiv 2\pi/\omega$ ),  $n = 0, 1, 2, \dots$ , yields

$$E(nT + T/2) = E(nT) - \delta \int_{nT}^{nT+T/2} \dot{x}^2(t) dt + \int_{nT}^{nT+T/2} \dot{x} \cos(x) \sin[\gamma \cos(\omega t)] dt + 2 \int_{nT}^{nT+T/2} \dot{x} \sin(x) \sin^2\left[\frac{\gamma}{2} \cos(\omega t)\right] dt. \quad (11)$$

Next, one applies the *first mean value theorem* [13] to the last integral in Eq. (11) to obtain

$$\frac{T}{4} \dot{x}(t^*) \sin[x(t^*)] [1 - J_0(\gamma)], \quad (12)$$

where  $J_n(\gamma)$ ,  $n = 0, 1, 2, \dots$  is the Bessel function of the first kind while  $t^* \in [nT, nT + T/2]$ . After using the Fourier series of  $\sin[\gamma \cos(\omega t)]$ , the second integral in Eq. (11) reads

$$2 \sum_{k=0}^{\infty} (-1)^k J_{2k+1}(\gamma) \times \int_{nT}^{nT+T/2} \dot{x} \cos(x) \cos[(2k+1)\omega t] dt. \quad (13)$$

After integrating by parts the integrals in Eq. (13) and applying again the first mean value theorem to the first (for  $k = 0$ ) of remaining integrals [notice that this theorem cannot be directly applied to the second integral in Eq. (11)], Eq. (13) becomes

$$4J_1(\gamma) \sin[x(t^*)] - \{\sin[x(nT + T/2)] + \sin[x(nT)]\} \sin(\gamma) + 2\omega \sum_{k=1}^{\infty} (-1)^k (2k+1) J_{2k+1}(\gamma) \times \int_{nT}^{nT+T/2} \sin(x) \sin[(2k+1)\omega t] dt, \quad (14)$$

with  $t^* \in [nT, nT + T/2]$  and where the relationship  $\sin(\gamma) = 2 \sum_{k=0}^{\infty} (-1)^k J_{2k+1}(\gamma)$  has been used [13]. Given the behavior of the Bessel functions  $J_{2k+1}(\gamma)$ ,  $k \geq 1$ , and the rapidly oscillating integrands of the integrals in Eq. (14) as  $k$  is increased from 1, one can neglect such integrals. Thus, putting everything together, Eq. (11) can be recast into the form

$$E(nT + T/2) = E(nT) - \delta \int_{nT}^{nT+T/2} \dot{x}^2(t) dt + \frac{T}{2} \dot{x}(t^*) \sin[x(t^*)] [1 - J_0(\gamma)] + 4J_1(\gamma) \sin[x(t^*)] - \{\sin[x(nT + T/2)] + \sin[x(nT)]\} \sin(\gamma). \quad (15)$$

In light of Eq. (15), the following observation is in order. Let us assume that, for fixed values of  $T$  and  $\delta$ , the dynamics is chaotic for a certain value of the amplitude,  $\gamma_{\text{chaos}}$ , which implies that  $E(nT + T/2) - E(nT) \geq 0$  for some values of  $n$ . This particular amplitude determines the values of the amplitude functions  $1 - J_0(\gamma_{\text{chaos}})$ ,  $J_1(\gamma_{\text{chaos}})$ , and  $\sin(\gamma_{\text{chaos}})$ . Now the possibility of suppressing or diminishing the chaos existing at  $\gamma = \gamma_{\text{chaos}}$  appears when one changes the amplitude  $\gamma$  such that at least one of the amplitude functions  $1 - J_0(\gamma)$ ,  $J_1(\gamma)$ ,  $\sin(\gamma)$  decreases with respect to its respective value of  $1 - J_0(\gamma_{\text{chaos}})$ ,  $J_1(\gamma_{\text{chaos}})$ , and  $\sin(\gamma_{\text{chaos}})$ . Clearly, the probability of suppressing the chaos existing for  $\gamma = \gamma_{\text{chaos}}$  is maximal at the zeros of  $J_1(\gamma)$  and  $\sin(\gamma)$  since the function  $1 - J_0(\gamma)$  does not present zeros for  $\gamma > 0$ . It is worth mentioning that this prediction is subject to the caveat that it is not expected to be uniformly valid for all values of the vibrating potential period because of its dependence on the integration domain [cf. Eq. (15)]. Numerical simulations confirmed its accuracy over significant ranges of the vibrating potential period, as can be seen in the illustrative instance shown in Fig. 3. One sees indeed that the widest regularization windows in the

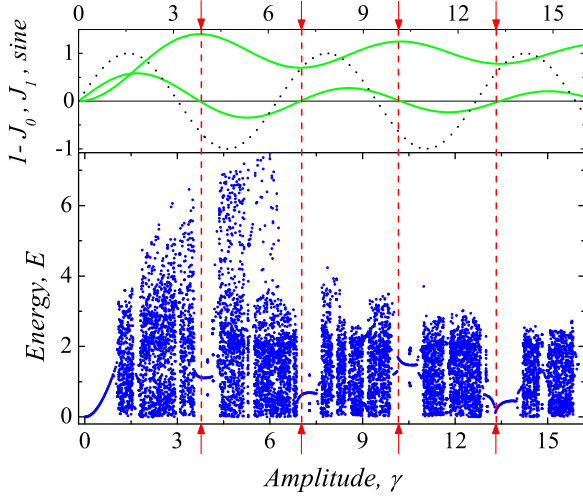


FIG. 3. (Color online) Top panel: Functions  $1 - J_0$  (upper line),  $J_1$ , and sine (dotted line) vs  $\gamma$  with  $J_{0,1}$  being Bessel functions of the first kind. Bottom panel: Bifurcation diagram of energy  $E$  as a function of the excitation amplitude  $\gamma$  for  $\delta = 0.1$  and  $\omega = 0.67$ . Vertical arrows indicate the four first zeros, 3.83, 7.02, 10.17, 13.32, of the Bessel function  $J_1(\gamma)$ . The quantities plotted are dimensionless.

bifurcation diagram of energy versus amplitude appear around and only around (all) the zeros of the function  $J_1(\gamma)$  over the range of amplitudes considered.

### III. CHAOS-CONTROL SCENARIO

Let us study now the suppressory effectiveness of a resonant external excitation  $F(t) \equiv \eta\gamma \cos(\omega t + \varphi)$  on the chaotic dynamics of Eq. (1):

$$\ddot{x} + \sin[x - \gamma \cos(\omega t)] = -\delta\dot{x} + \eta\gamma \cos(\omega t + \varphi), \quad (16)$$

which is equivalent to

$$\begin{aligned} \ddot{\theta} + \sin\theta &= -\delta\dot{\theta} + \delta\gamma\omega \sin(\omega t) \\ &+ \gamma\omega^2 \cos(\omega t) + \eta\gamma \cos(\omega t + \varphi) \end{aligned} \quad (17)$$

in the vibrating potential frame, and where  $\eta$  is an amplitude factor accounting for the relative amplitude of the two excitations involved while  $\varphi$  is the phase difference between them. After assuming that Eqs. (16) and (17) exhibit chaotic dynamics in the absence of any CS excitation ( $\eta = 0$ ) for a fixed set of parameters  $\{\delta, \gamma, \omega\}$ , one wishes to obtain analytical estimates of the regularization regions in the  $\varphi$ - $\eta$  parameter plane where the chaotic dynamics is suppressed.

#### A. Melnikov's method predictions

The application of MM to Eq. (17) yields the MF

$$\begin{aligned} M^\pm(t_0) &= -D \pm A \cos(\omega t_0) \pm B \sin(\omega t_0) \\ &\pm C \cos(\omega t_0 + \varphi), \\ C &\equiv 2\pi\eta\gamma \operatorname{sech}(\pi\omega/2), \end{aligned} \quad (18)$$

where the functions  $D, A, B$  are given by Eq. (6). In the following, it is assumed that a homoclinic bifurcation occurs in the absence of any CS excitation ( $\eta = 0$ ) such that the

condition (9) is satisfied, while the effectiveness of the CS excitation ( $\eta > 0$ ) at frustrating such a homoclinic bifurcation will be examined by considering for example the MF  $M^+(t_0)$  [the analysis of  $M^-(t_0)$  is similar and leads to the same conclusions]. To this end, it is convenient to use the normalized MF  $M_n^+(t_0) \equiv M^+(t_0)/D$  to write

$$\begin{aligned} M_n^+(t_0) &= -1 + (R + R'' \cos \varphi) \cos(\omega t_0) \\ &+ (R' - R'' \sin \varphi) \sin(\omega t_0) \\ &\leq -1 + \sqrt{(R + R'' \cos \varphi)^2 + (R' - R'' \sin \varphi)^2}, \end{aligned} \quad (19)$$

where  $R \equiv A/D, R' \equiv B/D, R'' \equiv C/D$ . If one now lets the CS excitation act on the system such that

$$(R + R'' \cos \varphi)^2 + (R' - R'' \sin \varphi)^2 \leq 1, \quad (20)$$

then this relationship represents a sufficient condition for  $M_n^+(t_0)$  to be negative (or null) for all  $t_0$ . The equals sign in Eq. (20) yields the boundary of the region in the  $\varphi$ - $\eta$  plane where homoclinic chaos is suppressed:

$$\begin{aligned} \eta &= \omega^2 \cos \varphi - \delta\omega \sin \varphi \\ &\pm \sqrt{\frac{\gamma_{\text{th}}^2}{\gamma^2} (\omega^4 + \omega^2 \delta^2) - (\omega^2 \sin \varphi + \delta\omega \cos \varphi)^2}, \end{aligned} \quad (21)$$

with  $\gamma > \gamma_{\text{th}}$  [cf. Eq. (9)], and where the two signs before the square root correspond to the two branches of the boundary. The following remarks may now be in order. First, the boundary function (21) represents a loop encircling the regularization region in the  $\varphi$ - $\eta$  plane which is symmetric with respect to the optimal suppressory values  $\varphi_{\text{opt}}$ , i.e., that value of the phase difference for which the range of suitable suppressory values of  $\eta$  is maximum. Second, in contrast to the chaos-control scenario for systems subjected to steady potentials, where the optimal suppressory values of the phase difference are constants which do not depend upon the remaining parameters [8], in the present case one straightforwardly obtains [cf. Eq. (21); see Fig. 4]

$$\varphi_{\text{opt}} = \varphi_{\text{opt}}(\delta/\omega) \equiv -\arctan(\delta/\omega). \quad (22)$$

Keeping  $\omega$  fixed, one thus obtains the limiting values

$$\lim_{\delta \rightarrow 0} \varphi_{\text{opt}} = \pi, \quad \lim_{\delta \rightarrow \infty} \varphi_{\text{opt}} = \pi/2. \quad (23)$$

This dependence of  $\varphi_{\text{opt}}$  on the ratio  $\delta/\omega$  represents a genuine feature of the chaos-control scenario associated with nonsteady potentials, being ultimately a consequence of the fact that there exist two reference frames involved in the description of the dynamics. Third, the regularization areas shrink as the ratio  $\gamma_{\text{th}}/\gamma$  diminishes, which means that the chaos-control scenario is *sensitive* to the strength of the initial chaotic state in the sense of its proximity to the threshold condition (9).

#### B. Energy-based analysis

By analyzing the variation in the system's energy in the vibrating potential frame, one can obtain additional theoretical confirmation of the main authentic feature of the above chaos-control scenario. Indeed, Eq. (17) has the associated energy

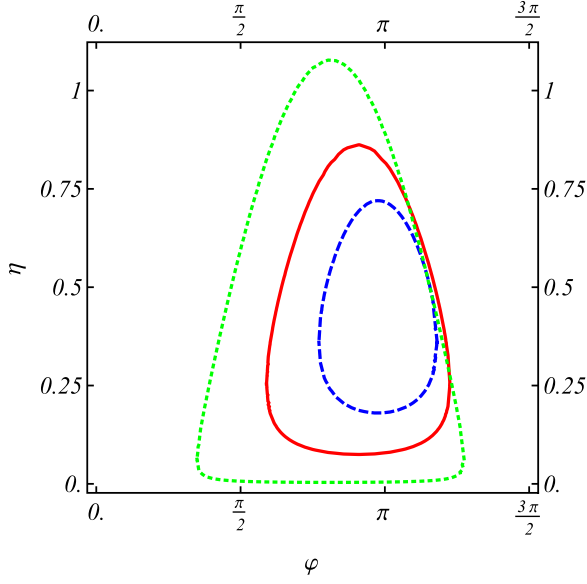


FIG. 4. (Color online) Generic boundary function [cf. Eq. (21)] encircling the region where homoclinic bifurcations are frustrated in the suppressory  $\varphi$ - $\eta$  parameter plane for three values of the damping coefficient:  $\delta = 0.05$  (dashed line),  $\delta = 0.2$  (solid line), and  $\delta = 0.45$  (dotted line). Fixed parameters:  $\gamma = 1.75, \omega = 0.67$ .

equation

$$\begin{aligned} \dot{E}_V = & -\delta \dot{\theta}^2 + \delta \gamma \omega \dot{\theta} \sin(\omega t) \\ & + \gamma \omega^2 \dot{\theta} \cos(\omega t) + \eta \gamma \dot{\theta} \cos(\omega t + \varphi), \end{aligned} \quad (24)$$

where  $E_V(t) \equiv (1/2)\dot{\theta}^2(t) + U[\theta(t)]$  [ $U(\theta) \equiv 1 - \cos \theta$ ] is the energy function in the vibrating potential frame. By introducing a new parameter  $\psi$  by means of the definitions

$$\sin \psi = -\frac{\delta}{\sqrt{\delta^2 + \omega^2}}, \quad \cos \psi = \frac{\omega}{\sqrt{\delta^2 + \omega^2}}, \quad (25)$$

one can conveniently recast Eq. (24) into the form

$$\begin{aligned} \dot{E}_V = & -\delta \dot{\theta}^2 + \eta \gamma \dot{\theta} \cos(\omega t + \varphi) \\ & + \gamma \omega \sqrt{\delta^2 + \omega^2} \dot{\theta} \cos(\omega t + \psi). \end{aligned} \quad (26)$$

Integration of Eq. (26) over any interval  $[nT, nT + T/2]$ ,  $n = 0, 1, 2, \dots$ , yields

$$\begin{aligned} E_V(nT + T/2) = & E_V(nT) - \delta \int_{nT}^{nT+T/2} \dot{\theta}^2(t) dt \\ & + \gamma \eta \int_{nT}^{nT+T/2} \dot{\theta}(t) \cos(\omega t + \varphi) dt \\ & + \gamma \omega \sqrt{\delta^2 + \omega^2} \int_{nT}^{nT+T/2} \dot{\theta}(t) \cos(\omega t + \psi) dt. \end{aligned} \quad (27)$$

Next, one applies the first mean value theorem to the last two integrals in Eq. (27) to finally obtain, after some simple

algebra,

$$\begin{aligned} E_V(nT + T/2) = & E_V(nT) - \delta \int_{nT}^{nT+T/2} \dot{\theta}^2(t) dt \\ & - \frac{\gamma T}{\pi} \dot{\theta}(t^*) (\omega \sqrt{\delta^2 + \omega^2} \sin \psi + \eta \sin \varphi) \\ & + 2\gamma \theta(t^{**}) (\omega \sqrt{\delta^2 + \omega^2} \cos \psi + \eta \cos \varphi) \\ & - \gamma [\theta(nT + T/2) + \theta(nT)] \\ & \times (\omega \sqrt{\delta^2 + \omega^2} \cos \psi + \eta \cos \varphi), \end{aligned} \quad (28)$$

with  $t^*, t^{**} \in [nT, nT + T/2]$ . Let us assume now that, in the absence of any CS excitation ( $\eta = 0$ ) and keeping fixed the values of  $T$  and  $\delta$ , the dynamics is chaotic for a certain value of the amplitude,  $\gamma_{\text{chaos}}$ , which implies that  $E_V(nT + T/2) - E_V(nT) \geq 0$  for some values of  $n$ . For  $\eta > 0$ , the possibility of suppressing or diminishing the chaos existing at  $\gamma = \gamma_{\text{chaos}}$  appears when the factors  $(\omega \sqrt{\delta^2 + \omega^2} \sin \psi + \eta \sin \varphi)$  and  $(\omega \sqrt{\delta^2 + \omega^2} \cos \psi + \eta \cos \varphi)$  in Eq. (28) decrease with respect to their respective values for  $\eta = 0$ . Clearly, the probability of suppressing the chaos existing for  $\gamma = \gamma_{\text{chaos}}$  is maximal when such factors vanish, thus providing the optimal suppressory value of the phase difference:

$$\begin{aligned} \sin \varphi_{\text{opt}} = \omega \delta / \eta \geq 0 & \iff \varphi_{\text{opt}} \in [0, \pi], \\ \cos \varphi_{\text{opt}} = -\omega^2 / \eta < 0 & \iff \varphi_{\text{opt}} \in ]\pi/2, 3\pi/2[, \\ \varphi_{\text{opt}} = -\arctan(\delta / \omega). \end{aligned} \quad (29)$$

Thus, one again obtains the aforementioned authentic feature predicted from MM,  $\varphi_{\text{opt}} = \varphi_{\text{opt}}(\delta / \omega)$ , and hence the limiting values  $\lim_{\delta \rightarrow 0} \varphi_{\text{opt}} = \pi$ ,  $\lim_{\delta \rightarrow \infty} \varphi_{\text{opt}} = \pi/2$  [cf. Eqs. (22) and (23)].

### C. Numerical results

One can compare the theoretical results obtained from the MM (and energy analysis) and LE calculations of the model system (16). We computed LEs by integrating Eq. (16) typically up to  $10^4$  drive cycles for each fixed set of parameters. The numerical results confirmed the effectiveness of the estimate (21). In the absence of the CS excitation ( $\eta = 0$ ), the model system (16) with  $\delta = 0.1, \gamma = 1.4, \omega = 0.67$  exhibits a strange chaotic attractor with a maximal LE  $\lambda^+(\eta = 0) = 0.114$ . The maximal LE was calculated for each point on a  $100 \times 100$  grid with phase difference  $\varphi$  and amplitude factor  $\eta$  along the horizontal and vertical axes. The results are shown in Fig. 5 (top), where the diagram was constructed by only plotting points on the grid according to a color code when the respective LE was greater than  $10^{-3}$  and with a dashed black contour denoting the theoretical boundary function [cf. Eq. (21)]. One sees that complete regularization [ $\lambda^+(\eta > 0) \leq 0$ ] mainly appears inside the maximal island which symmetrically contains the theoretically predicted area where even the chaotic transients are eliminated. A second instance is shown in Fig. 5 (bottom) for the fixed parameters  $\delta = 0.255, \gamma = 1.75, \omega = 0.67$  and the model system (16) exhibiting a strange chaotic attractor with a maximal LE  $\lambda^+(\eta = 0) = 0.122$ . A comparison of Figs. 5 [(top) and (bottom)] nicely confirms that the deviation of the optimal

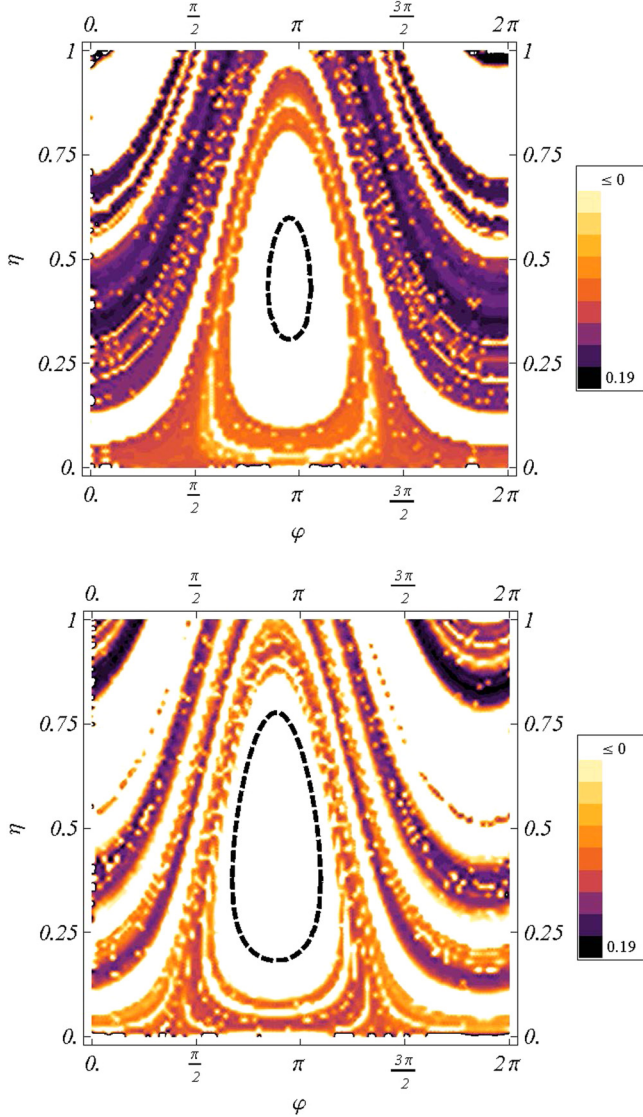


FIG. 5. (Color online) Maximal LE in the  $\varphi$ - $\eta$  parameter plane for  $(\delta, \gamma) = (0.1, 1.4)$  (top panel) and  $(\delta, \gamma) = (0.255, 1.75)$  (bottom panel). The dashed black contours indicate the predicted boundary functions [cf. Eq. (21)] which are symmetric with respect to the optimal suppressory values of the phase difference. Fixed frequency:  $\omega = 0.67$ . The quantities plotted are dimensionless.

phase difference from its limiting value  $\pi$  [cf. Eq. (23)] increases as the damping coefficient is increased from 0.

Regarding the regularization routes, one typically finds frequency-locked behavior inside the main regularization island. Figure 6 shows bifurcation diagrams (energy  $E$  versus phase difference  $\varphi$ ) constructed by means of a Poincaré map for  $\omega = 0.67, \eta = 0.4$ , and two sets of the remaining parameters. Starting at  $\varphi = 0$ , and taking the transient time as  $500T$  after every increment of  $\Delta\varphi = \pi/300$ , we sampled 20 excitation periods by picking up the first  $E$  value of each excitation cycle. The same initial conditions were set for every  $\varphi$  after  $\Delta\varphi$  was added. The theoretical suppressory ranges are indicated for comparison with the respective numerically obtained ranges of suppression of chaos. We found that steady responses inside the theoretical suppressory ranges are systematically

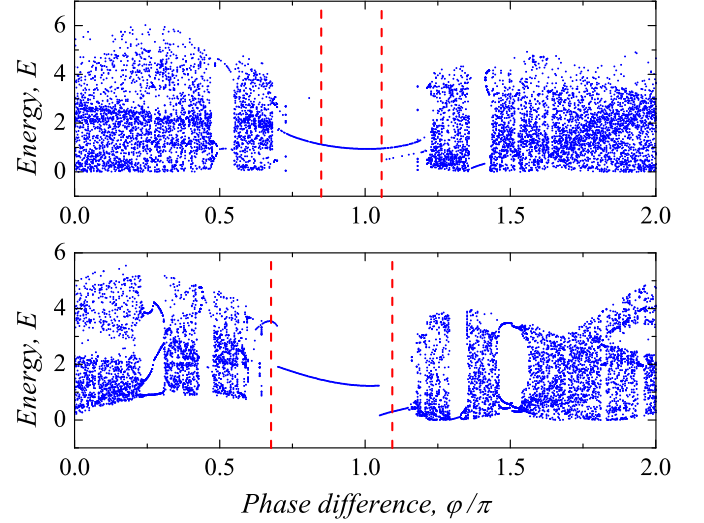


FIG. 6. (Color online) Bifurcation diagrams of the energy  $E$  as a function of the phase difference  $\varphi$  for  $\omega = 0.67, \eta = 0.4$ , and two sets of the remaining parameters:  $(\delta, \gamma) = (0.1, 1.4)$  (top panel),  $(\delta, \gamma) = (0.255, 1.75)$  (bottom panel). Vertical dashed lines delimit the ranges corresponding to the predicted boundary functions [cf. Eq. (21)]. The quantities plotted are dimensionless.

period-1 attractors which are reached as  $\varphi \rightarrow \varphi_{\text{opt}}$  through a fairly rich route including crises and inverse period-doubling bifurcations. A comparison of Figs. 6 [(top) and (bottom)] shows again how the deviation of the optimal phase difference from its limiting value  $\pi$  [cf. Eq. (23)] increases as the damping coefficient is increased.

Next, we assume a subharmonic resonance condition  $\Omega = n\omega, n = 1, 2, 3, \dots$ , in the CS excitation  $F(t) \equiv \eta\gamma \cos(\Omega t + \varphi)$  [cf. Eq. (1) with  $f(t) = \gamma \cos(\omega t)$ ] to study the relative suppressory effectiveness of the main resonance ( $n = 1$ ) with respect to higher-order subharmonic resonances ( $n > 1$ ). One typically finds that the main resonance is the most effective resonance in the sense that it provides the widest phase difference intervals where chaos is suppressed for a fixed choice of the remaining parameters. Figure 7 shows an illustrative example for the subharmonic resonances  $n = \{2, 3, 4\}$  while a comparison of Figs. 6 (top) and 7 clearly confirms the superior effectiveness of the main resonance.

### 1. Robustness against additive Gaussian noise

Since noise is unavoidable and significant in many physical contexts, including many nanoscale devices, it is pertinent and relevant to study the robustness of the present chaos-control scenario against the presence of additive noise:

$$\ddot{x} + \sin[x - \gamma \cos(\omega t)] = -\delta\dot{x} + \eta\gamma \cos(\omega t + \varphi) + \sqrt{\sigma}\xi(t), \quad (30)$$

where  $\xi(t)$  is a Gaussian white noise with zero mean and  $\langle \xi(t)\xi(t+s) \rangle = \delta_D(s)$ , with  $\delta_D(s)$  being the Dirac  $\delta$ , while  $\sigma = 2\delta k_b T$  with  $k_b$  and  $T$  being the Boltzmann constant and temperature, respectively. To study numerically the effect of noise on the purely deterministic chaos-control scenario, we calculated the maximal LE on averaging over different realizations of noise,  $\langle \lambda^+ \rangle$ , and compare it with that of the

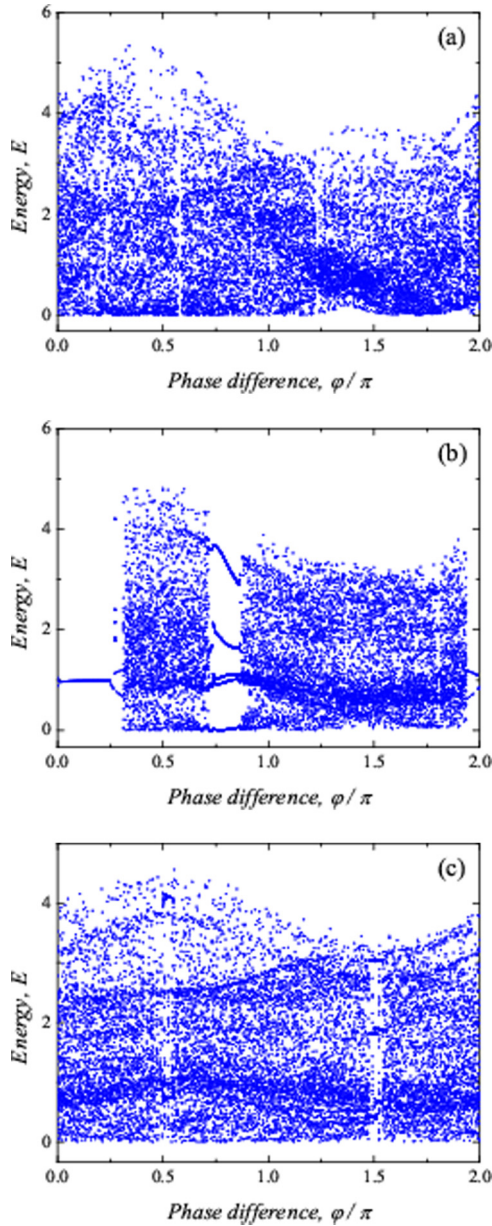


FIG. 7. (Color online) Bifurcation diagrams of the energy  $E$  as a function of the phase difference  $\varphi$  for  $\delta = 0.1, \gamma = 1.4, \omega = 0.67, \eta = 0.4$ , and three different values of the CS frequency (see the text):  $\Omega = 2\omega$  (a),  $\Omega = 3\omega$  (b), and  $\Omega = 4\omega$  (c). The quantities plotted are dimensionless.

purely deterministic case. In the absence of any CS excitation ( $\eta = 0$ ) the strength of the purely deterministic chaotic behavior monotonously decreases as the noise intensity is increased from 0, as is shown in the example of Fig. 8. In the presence of CS excitations ( $\eta > 0$ ) one typically obtains a shrinkage of the regularization regions in parameter space with respect to the purely deterministic case. Figure 9 shows the averaged maximal LE in the  $\varphi$ - $\eta$  parameter plane for two values of the noise intensity:  $\sigma = 0.00459$  [Fig. 9 (top)] and  $\sigma = 0.0153$  [Fig. 9 (bottom)], and the same remaining parameters as in the purely deterministic case shown in Fig. 5 (bottom). A comparison of Figs. 9 and 5 (bottom) clearly confirms the

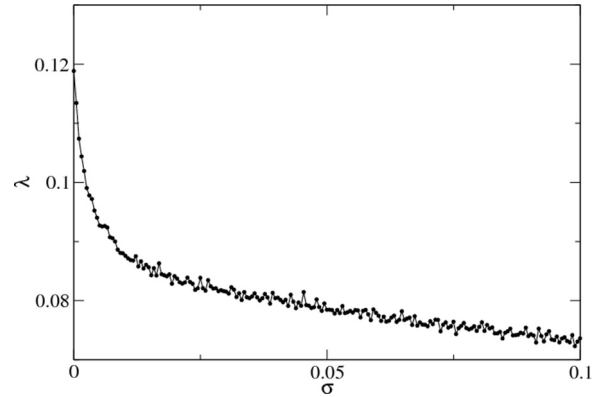


FIG. 8. Maximal LE (see the text) versus noise intensity for the noisy system [cf. Eq. (30)] with  $\delta = 0.255, \gamma = 1.75, \omega = 0.67$ , and  $\eta = 0$ . The quantities plotted are dimensionless.

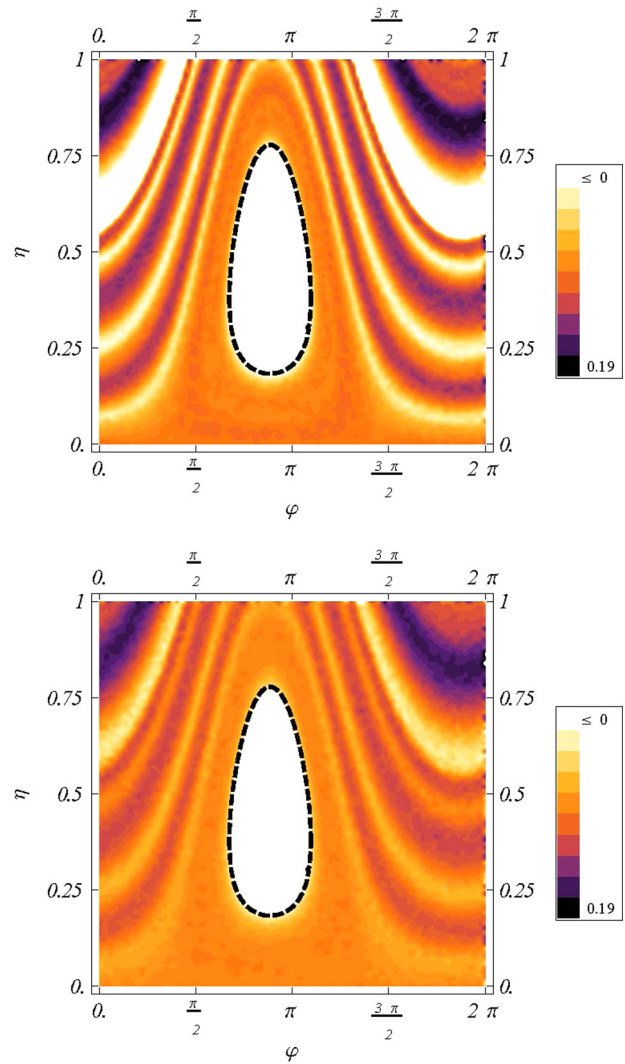


FIG. 9. (Color online) Maximal LE (see the text) in the  $\varphi$ - $\eta$  parameter plane for  $\delta = 0.255, \gamma = 1.75, \omega = 0.67$ , and two values of the noise intensity:  $\sigma = 0.00459$  (top panel) and  $\sigma = 0.0153$  (bottom panel). The dashed black contour indicate the predicted boundary function for the purely deterministic case [ $\sigma = 0$ , cf. Eq. (21)]. The quantities plotted are dimensionless.

robustness of the CS excitation in suppressing chaos against noise. In particular, one sees that the maximum suppression of chaos is achieved for the same optimal suppressory value of  $\varphi$  than that corresponding to the purely deterministic case ( $\sigma = 0$ ). Remarkably, the most robust region in the suppressory  $\varphi$ - $\eta$  parameter plane is precisely that encircled by the theoretical boundary function corresponding to the purely deterministic case [cf. Eq. (21), see Fig. 9 (bottom)].

## 2. Robustness against reshaping of CS excitations

Next, we briefly study the robustness of the chaos-control scenario against reshaping of the CS excitation by considering the generalized systems:

$$\ddot{x} + \sin[x - \gamma \cos(\omega t)] = -\delta \dot{x} + \eta \gamma \operatorname{sn}(\Omega t + \Phi; m), \quad (31)$$

$$\ddot{x} + \sin[x - \gamma \cos(\omega t)] = -\delta \dot{x} + \eta \gamma \operatorname{cn}(\Omega t + \Phi; m), \quad (32)$$

where all variables and parameters are dimensionless. Here,  $\operatorname{cn}(\cdot; m)$ ,  $\operatorname{sn}(\cdot; m)$  are Jacobian elliptic functions of parameter  $m \in [0, 1]$ ,  $\Omega = \Omega(m, T) \equiv 4K(m)/T$ , and  $\Phi = \Phi(m, T) \equiv 2K(m)\varphi/\pi$ ,  $\varphi \in [0, 2\pi]$ , where  $K(m)$  is the complete elliptic integral of the first kind (see, e.g., Refs. [13, 14]). When  $m = 0$ , one has

$$\begin{aligned} \operatorname{sn}(\Omega t + \Phi; m = 0) &= \cos(\omega t + \varphi - \pi/2), \\ \operatorname{cn}(\Omega t + \Phi; m = 0) &= \cos(\omega t + \varphi), \end{aligned} \quad (33)$$

i.e., one recovers the case of a harmonic CS excitation. In the other limit,

$$\operatorname{sn}(\Omega t + \Phi; m = 1) = \frac{4}{\pi} \sum_{n=1}^{\infty} \frac{\sin[(2n-1)(\omega t + \varphi)]}{2n-1}, \quad (34)$$

which is the square-wave function of period  $T$ . The effect of renormalization of the elliptic sine-cosine argument is clear: With  $T$  constant, solely the excitation shape is varied by increasing the shape parameter  $m$  from 0 to 1 (see Fig. 10). There is thus a smooth transition from a sine function to a square wave for the elliptic sine  $\operatorname{sn}(\Omega t + \Phi; m)$ . Since the elliptic cosine  $\operatorname{cn}(\Omega t + \Phi; m)$  represents a periodic string of symmetric pulses, whose effective width decreases as  $m$  increases from  $m = 0$ , in the limiting value  $m = 1$  the string vanishes, i.e., one recovers Eq. (3) (absence of any CS excitation). This allows one to study the genuine effect on the chaos-control scenario of reshaping the CS excitation [cf. Eqs. (16), (31), and (32)]. Some illustrative examples for the case of an elliptic sine (cosine) excitation are given in Fig. 11 (12) where we show bifurcation diagrams (energy  $E$  versus phase difference  $\varphi$ ) for the same four values of the shape parameter as in Fig. 10:  $m = 0$ ,  $0.99$ ,  $1 - 10^{-8}$ ,  $1 - 10^{-14}$ . In the case of the elliptic sine excitation [see Fig. 10 (top)], we obtain that the regularization scenario remains the same as the excitation shape is varied from a sine function [Fig. 11(a)] to a square wave [Fig. 11(d)]. Notice that the widest regularization window is symmetric with respect to the optimal value  $\varphi_{\text{opt}} \simeq \pi/2 + \pi = 3\pi/2$ , as expected from Eqs. (23) and (33). In the case of the elliptic cosine excitation [see Fig. 10 (bottom)], we obtain that the

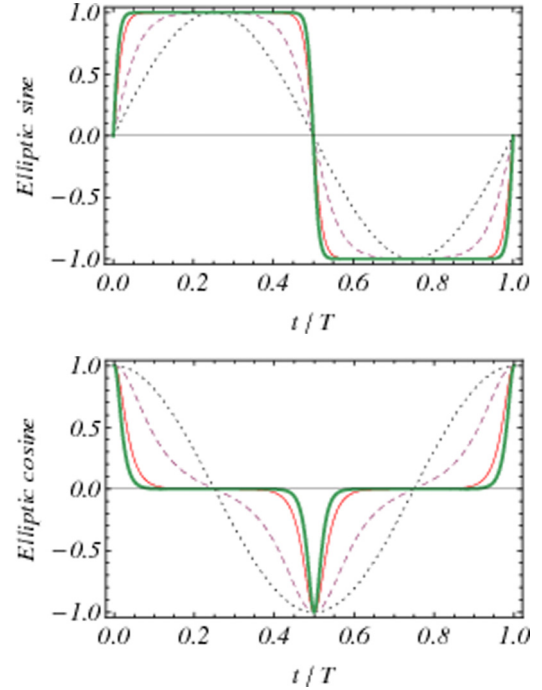


FIG. 10. (Color online) Plots of the functions  $\operatorname{sn}[4K(m)t/T; m]$  (elliptic sine, top panel) and  $\operatorname{cn}[4K(m)t/T; m]$  (elliptic cosine, bottom panel) for  $m = 0$  (dotted line),  $0.99$  (dashed line),  $1 - 10^{-8}$  (thin line), and  $1 - 10^{-14}$  (thick line).

regularization scenario remains the same for sufficiently wide pulses, as for  $m = 0$  [Fig. 12(a)] and  $m = 0.99$  [Fig. 12(b)], for which the widest regularization window is symmetric with respect to the optimal value  $\varphi_{\text{opt}} \simeq \pi$ , as expected from Eqs. (23) and (33). This main regularization window is no longer maintained for sufficiently narrow pulses, as for  $m = 1 - 10^{-8}$  [Fig. 12(c)], for which one sees the appearance

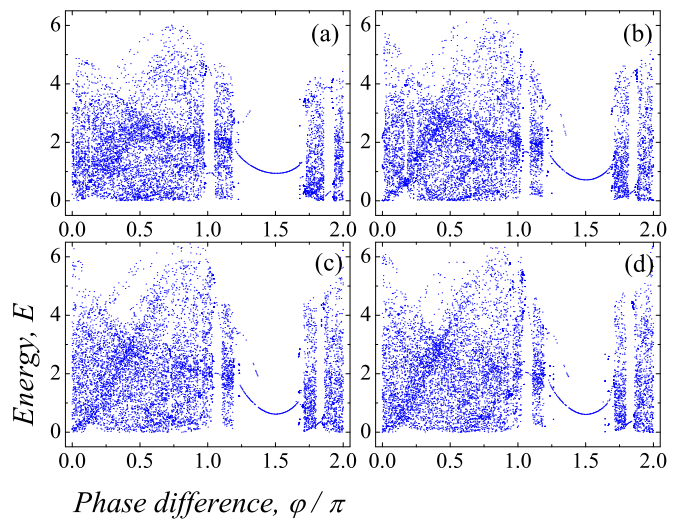


FIG. 11. (Color online) Bifurcation diagrams of the energy  $E$  as a function of the phase difference  $\varphi$  for a CS excitation given by an elliptic sine [Eq. (31)] with  $\delta = 0.1$ ,  $\gamma = 1.4$ ,  $\omega = 0.67$ ,  $\eta = 0.4$ , and four values of the shape parameter:  $m = 0$  (a),  $m = 0.99$ , (c)  $m = 1 - 10^{-8}$ , and (d)  $m = 1 - 10^{-14}$ . The quantities plotted are dimensionless.

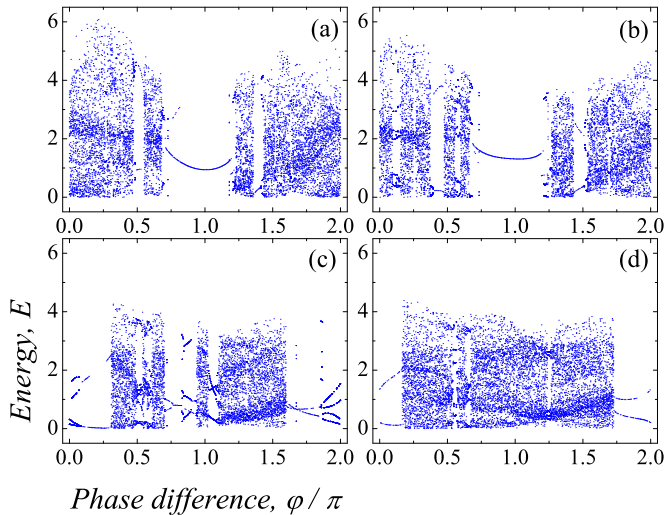


FIG. 12. (Color online) Bifurcation diagrams of the energy  $E$  as a function of the phase difference  $\varphi$  for a CS excitation given by an elliptic cosine [Eq. (32)] with  $\delta = 0.1, \gamma = 1.4, \omega = 0.67, \eta = 0.4$ , and four values of the shape parameter:  $m = 0$  (a),  $m = 0.99$ , (c)  $m = 1 - 10^{-8}$ , and (d)  $m = 1 - 10^{-14}$ . The quantities plotted are dimensionless.

of new noticeable regularization windows. For even narrower pulses, as for  $m = 1 - 10^{-14}$  [Fig. 12(d)], the regularization windows are ever narrower as  $m \rightarrow 1$ , as expected from the behavior of the elliptic cosine as  $m \rightarrow 1$  [see Fig. 10 (bottom)]. An exhaustive study of the suppressory effect of general (nonharmonic) CS excitations is beyond the scope of the present work and further analysis will be given elsewhere.

#### IV. CONCLUSION

In this paper we have studied both theoretically and numerically the dissipative chaotic dynamics of a paradigmatic model in which a damped particle is subjected to a horizontally and harmonically vibrating periodic potential. The effectiveness of an added harmonic external excitation which is in resonance with the vibrating potential at suppressing the chaos existing in its absence was predicted theoretically and then confirmed numerically. The phase difference between the two harmonic excitations involved was shown to play a crucial role in the

chaos-control scenario, with the special feature that its optimal value depends upon the ratio between the damping coefficient and the excitation frequency. This represents an authentic feature of the chaos-control scenario associated with nonsteady potentials which is in contrast to the steady potential case, in which the optimal suppressory values of the phase difference are constants which do not depend upon the remaining parameters [8,15–17]. Also, we found that the present chaos-control scenario is robust against the presence of low-intensity Gaussian noise, thus allowing its potential application to small systems where the presence of thermal noise is unavoidable. Additionally, we provided numerical evidence of the robustness of the chaos-control scenario against the reshaping of chaos-suppressing excitations. Remarkably, the application of mean value theorems to analyzing the system's energy revealed how powerful these tools are at extracting useful information regarding the order-chaos threshold in parameter space regions in which Melnikov's method is inapplicable.

The present results may be directly applied to diverse physical contexts where the paradigmatic model described by Eq. (1) appears naturally while the chaotic dynamics is clearly undesirable, including, for example, setups of a noncontact rack-and-pinion type coupled by the lateral Casimir force [3] or the chaotic phase oscillations of a proton beam in a cooler synchrotron [1]. Some interesting open problems remain. Among them, the authors are presently considering the structural stability of the chaos-control scenario when the vibrating potential is subjected to generic (nonharmonic) periodic excitations and the chaos-suppressing external excitations are generic periodic functions, too. The effectiveness of the chaos-control scenario in the contexts of linear chains and scale-free networks points to additional interesting problems for future research.

#### ACKNOWLEDGMENTS

R.C. and J.A.M. acknowledge financial support from the Ministerio de Economía y Competitividad (MINECO, Spain) through Project No. FIS2012-34902 cofinanced by FEDER funds. R.C. acknowledges financial support from the Junta de Extremadura (JEx, Spain) through Project No. GR15146. P.J.M. acknowledge financial support from the Ministerio de Economía y Competitividad (MINECO, Spain) through Project No. FIS2011-25167 cofinanced by FEDER funds.

- 
- [1] M. Ellison *et al.*, *Phys. Rev. Lett.* **70**, 591 (1993).
  - [2] F. Li, W. Hai, Z. Ren, and W. Shu, *Phys. Lett. A* **355**, 104 (2006).
  - [3] A. Ashourvan, M. F. Miri, and R. Golestanian, *Phys. Rev. E* **75**, 040103(R) (2007).
  - [4] Y. Azizi and A. Valizadeh, *Phys. Rev. A* **83**, 013614 (2011).
  - [5] S. Longhi *et al.*, *Phys. Rev. Lett.* **96**, 243901 (2006).
  - [6] M. Glück, A. R. Kolovsky, and H. J. Korsch, *Phys. Rep.* **366**, 103 (2002).
  - [7] B. Liebchen and P. Schmelcher, *New J. Phys.* **17**, 083011 (2015).
  - [8] R. Chacón, *Control of Homoclinic Chaos by Weak Periodic Perturbations* (World Scientific, Singapore, 2005).
  - [9] D. McKay, M. White, M. Pasienski, and B. DeMarco, *Nature* **453**, 76 (2008).
  - [10] V. K. Melnikov, *Tr. Mosk. Ova.* **12**, 3 (1963) [Trans. Moscow Math. Soc. **12A**, 1 (1963)].
  - [11] J. Guckenheimer and P. Holmes, *Nonlinear Oscillations, Dynamical Systems, and Bifurcations of Vector Fields* (Springer-Verlag, New York, 1983).
  - [12] A. Wolf *et al.*, *Physica D (Amsterdam)* **16**, 285 (1985).
  - [13] M. Abramowitz and I. A. Stegun, *Handbook of Mathematical Functions* (Dover, New York, 1972).
  - [14] J. V. Armitage and W. F. Eberlein, *Elliptic Functions* (Cambridge University Press, Cambridge, England, 2006).
  - [15] S. Rajasekar, *Pramana J. Phys.* **41**, 295 (1993).
  - [16] R. Chacón, *Eur. Phys. J. B* **30**, 207 (2002).
  - [17] R. Chacón, *Philos. Trans. R. Soc. London A* **364**, 2335 (2006).